Supplementary Material

Analytical prediction at constant fall speed

The equations (2.12-2.14) of the main text are recalled here:

$$\langle \boldsymbol{x}_n \cdot \boldsymbol{x}_n \rangle = \langle \boldsymbol{x}_{n-1} \cdot \boldsymbol{x}_{n-1} \rangle + \frac{(1-\alpha)^2}{c_D^2} \langle \dot{\boldsymbol{x}}_{n-1} \cdot \dot{\boldsymbol{x}}_{n-1} \rangle + 2\frac{(1-\alpha)}{c_D} \langle \boldsymbol{x}_{n-1} \cdot \dot{\boldsymbol{x}}_{n-1} \rangle + \frac{c_L^2}{c_D^4} (\alpha - 1 + c_D)^2 , \quad [1]$$

$$\langle \dot{\boldsymbol{x}}_n \cdot \dot{\boldsymbol{x}}_n \rangle = \alpha^2 \langle \dot{\boldsymbol{x}}_{n-1} \cdot \dot{\boldsymbol{x}}_{n-1} \rangle + \frac{c_L^2}{c_D^2} (1-\alpha)^2 , \quad [2]$$

$$\langle \boldsymbol{x}_n \cdot \dot{\boldsymbol{x}}_n \rangle = \alpha \langle \boldsymbol{x}_{n-1} \cdot \dot{\boldsymbol{x}}_{n-1} \rangle + \frac{\alpha(1-\alpha)}{c_D} \langle \dot{\boldsymbol{x}}_{n-1} \cdot \dot{\boldsymbol{x}}_{n-1} \rangle + \frac{c_L^2}{c_D^3} (1-\alpha)(\alpha - 1 + c_D) , \quad [3]$$

where an ensemble average $\langle \ldots \rangle$ was performed over the many falling drops. Since Re, St and then c_D and c_L directly depend on the increasing fall speed v, the recurrence relations of Eqs (1-3) can only be solved numerically. We may nevertheless seek for an analytical solution at constant v, i.e. constant c_D and c_L.

The solution to Eqs (1-3) from initial rest conditions $\boldsymbol{x}_0 = \boldsymbol{0}$ and $\dot{\boldsymbol{x}}_0 = \boldsymbol{0}$ are:

$$\langle \dot{\boldsymbol{x}}_n \cdot \dot{\boldsymbol{x}}_n \rangle = \frac{c_L^2}{c_D^2} \frac{1-\alpha}{1+\alpha} \left(1 - \alpha^{2n}\right) , \quad [4]$$

$$\langle \boldsymbol{x}_n \cdot \dot{\boldsymbol{x}}_n \rangle = \frac{c_L^2}{c_D^3} \frac{1-\alpha^n}{1+\alpha} \left[(\alpha - 1)(1 + \alpha^n) + c_D (1+\alpha) \right], \quad [5]$$

$$\langle \boldsymbol{x}_n \cdot \boldsymbol{x}_n \rangle = \frac{n c_L^2}{c_D^2} + \frac{c_L^2}{c_D^4} \frac{(1-\alpha)\left(1-\alpha^{2n}\right)}{1+\alpha} - \frac{2c_L^2}{c_D^3} (1 - \alpha^n) . \quad [6]$$

This yields the dimensional standard deviation of drop distribution Δ:

$$\Delta = \sqrt{\langle \mathbf{x}_n \cdot \mathbf{x}_n \rangle} = vT \sqrt{\langle \boldsymbol{x}_n \cdot \boldsymbol{x}_n \rangle}. \quad [7]$$

The resulting curve at constant parameters is shown in Fig. S1, with $R = 2.64$ mm, $v_0 = 10.50$ m/s, $f = 300$ Hz, St$= 0.2$, $C_D = 0.48$ and $C_L = 0.067$.

Asymptotic behaviours. In the limit case where drag is completely neglected, namely when $nc_D << 1$ (or $\alpha^n \to 1$), which here approximately corresponds to a falling height $z_0 < 0.5$ m, the leading term of Eq. (6) is proportional to $c_L^2 n^3/3$. As $nc_D >> 1$ ($\alpha^n << 1$), corresponding here to $z_0 > 25$ m, the leading order becomes $c_L^2 n / c_D^2$. Between these two regions, which corresponds to the range of values covered experimentally, $\langle \mathbf{x}_n \cdot \mathbf{x}_n \rangle$ is thus in an intermediate regime that can be approximated as being proportional to n^2. Therefore, from Eq. (7), Δ increases linearly with n. Considering St, f and v as constant during the whole drop trajectory, n can be estimated proportional to z_0, hence Δ is more or less proportional to z_0 too in the range covered in cave and in lab, as observed in Fig. S1.

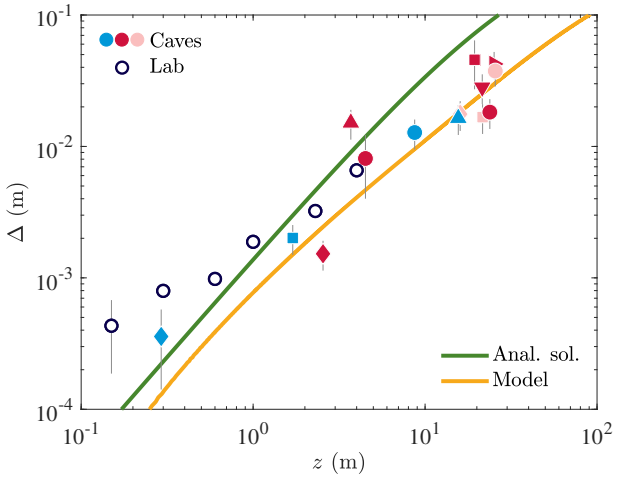

Fig. S1. Standard deviation Δ of impact point position as a function of the falling height z_0. The yellow solid curve is obtained by solving numerically the recurrence relations of Eqs (10) and (11) from the main text and varying parameters v, f, Re, St and C_D at each vortex emission. The lift coefficient C_L is set to 0.067, as an average across Reynolds of the RMS values found in the literature (see Table 1 from the main text). The green solid line corresponds to the analytical curve of Eq. (7) for $C_D = 0.48$ and $C_L = 0.067$. Hollow symbols ○ correspond to data obtained for drops of radius $R = 2.32$ mm in a lab setting. All the solid symbols (in red ●, pink ● and blue ●) represent experimental measurements obtained in caves with high-speed videos (cf. Table S1).

ANOVA test

An ANOVA test was performed for $r(\mathrm{We}, \delta^*)$ on data from 13 stalagmites. Both factors We and δ^* were split into three levels as indicated in the graphs of the next page: small, medium and large relative to the classical values found in situ. Hence, the three levels for We are: We ≤ 3500, $3500 <$ We ≤ 5500 and We > 5500. On the other hand, the levels chosen for δ^* are: $\delta^* \leq 0.015$, $0.015 < \delta^* \leq 0.030$ and $\delta^* > 0.030$.

The p-values returned by the test are: $p = 2.3 \times 10^{-4}$ for We, and $p = 0.1$ for δ^*. There is therefore a significant variation in r caused by the value of We, whereas variations with δ^* may not be statistically significant. However, the literature (see Main Text) indicates that the maximum size of the lamella r may only vary as a power of We close to 1/4. Considering the parameter r as a constant is thus a good first approximation.

Supplementary graphs: lamella maximum extension r as a function of Weber number and film thickness

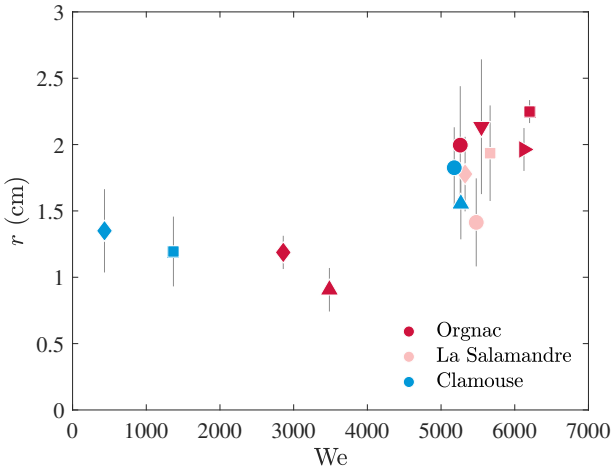

Fig. S2. Maximum radius r reached by the liquid lamella formed right after the drop impact on the stalagmite, as a function of the Weber number We attained by the drop right before impact. Each symbol corresponds to a specific stalagmite, as reported in Table S1.

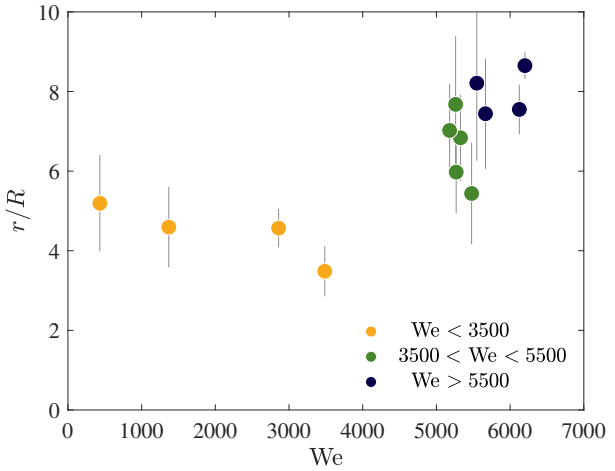

Fig. S3. Non-dimensional maximum radius r/R reached by the liquid lamella formed right after the drop impact on the stalagmite, as a function of the Weber number We attained by the drop right before impact. Three bins of δ^* were considered for the ANOVA test: yellow symbols ● represent impacts for We < 3500, green symbols ● correspond to impacts in the range $3500 <$ We < 5500 and dark blue ones ● to We > 5500.

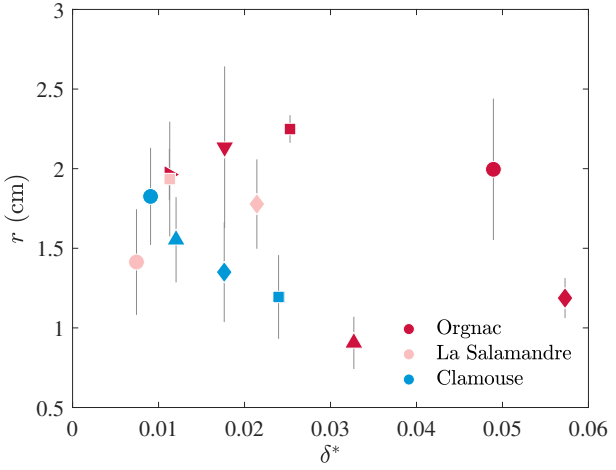

Fig. S4. Maximum radius r reached by the liquid lamella formed right after the drop impact on the stalagmite, as a function of the non-dimensional film thickness $\delta^* = \delta/R$, averaged over the top surface of the stalagmite. Each symbol corresponds to a specific stalagmite, as reported in Table S1.

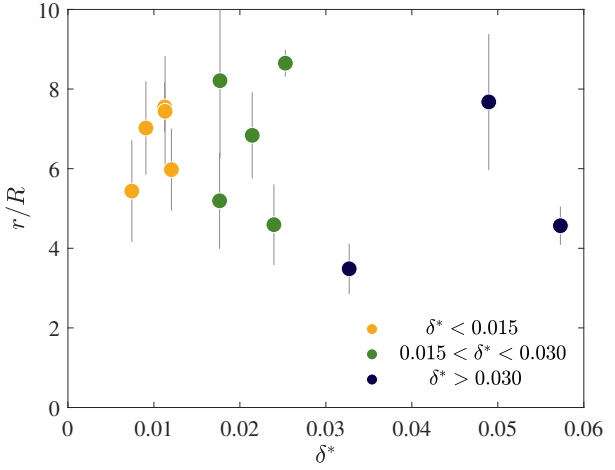

Fig. S5. Non-dimensional maximum radius r/R reached by the liquid lamella formed right after the drop impact on the stalagmite, as a function of the non-dimensional film thickness $\delta^* = \delta/R$, averaged over the top surface of the stalagmite. Three bins of δ^* were considered for the ANOVA test:: yellow symbols ● represent impacts for $\delta^* < 0.015$, green symbols ● correspond to impacts in the range $0.015 < \delta^* < 0.030$ and dark blue ones ● to $\delta^* > 0.030$.

Snapshot from supplementary video of a drop falling off a stalactite

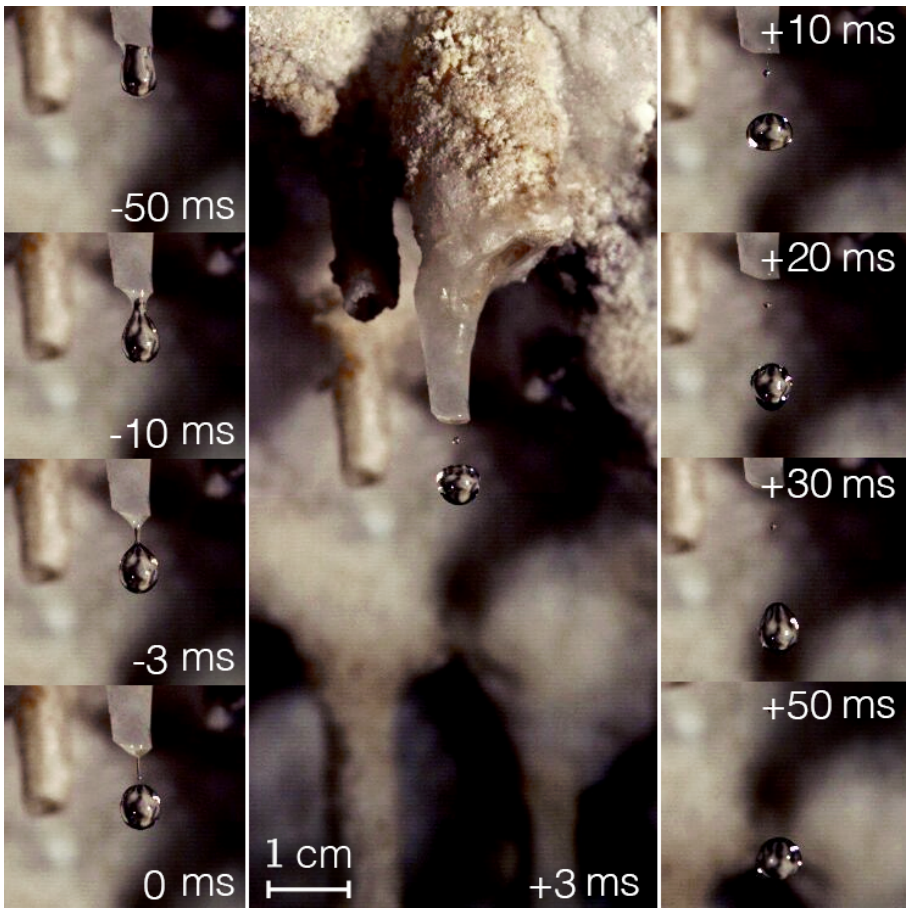

Fig. S6. Evolution of a growing pendant drop falling from a stalactite tip in Orgnac cave, salle de Joly. Pictures show the drop from at least 50 ms before it detaches to at most 50 ms after. The most pronounced shape variations of the drop appearing on the first few centimeters of its trajectory can be seen in the right-hand pictures.

Cave measurements

Cave	*Room* / Neighbouring concr.	Symbol	Name	Nb. videos	Date	z_0 (m)	δ (μm)	s_b (cm)	s_t (cm)	Table	Figure
Clamouse	*Salle rouge*	●	Clam01	50	06.16.16	8.70	50	5.84	3.16	S3	S7 A
	Cimetière	■	Clam02	50	06.16.16	1.70	125	3.21	1.85	S4	S7 B
	Cimetière	◆	Clam03	10	06.16.16	0.29	90	3.02	1.77	S5	S8 A
	Below Cimetière	▼	Clam04	49	06.16.16	15.60	60	7.83	3.55	S8	S8 B
Orgnac	Tour de Pise *(SJ)*	●	Org01	56	03.24.15 – 06.13.16	23.80	255	8.40	4.93	S9	S9 A
	Pomme de Pin *(SJ)*	■	Org02	27	03.25.15 – 06.13.16	19.40	130	8.98	5.03	S7	S10 A
	Near *salle Glory (SJ)*	◆	Org03	50	06.14.16	2.55	300	4.71	1.89	S10	S10 B
	Near *salle Petit* entrance *(SJ)*	▼	Org04	48	06.14.16	3.70	170	4.84	2.89	S11	S9 D
	Blocs Cyclopéens *(SJ)*	▲	Org05	50	06.14.16	21.50	90	8.55	5.12	S12	S9 B
	Cône d'Éboulis (*SJ*)	▶	Org06	42	06.14.16	25.20	60	10.59	6.42	S13	S9 C
	Salle Glory	◀	Org07	7	03.25.15	4.50	-	4.43	2.58	S6	S10 C
La Salamandre	Pomme de Pin	●	Sal01	43	06.15.16	25.60	40	8.07	5.50	S14	S11 A
	Cierges	■	Sal02	50	06.15.16	21.60	60	8.97	4.96	S15	S11 B
	Grands Massifs	◆	Sal03	50	06.15.16	16.00	110	7.29	4.19	S16	S11 C

Table S1: High-speed movie database. *From left to right.* Caves in which high-speed videos of drop impacts on stalagmites were recorded. Rooms in which stalagmites were filmed (indicated in *italic*, with *SJ* meaning *salle de Joly*) or important concretions in the neighbourhood of the filmed stalagmites. Symbols representing each filmed stalagmite in Fig. 3 and 4 of the main text. Names of these stalagmites. Number of high-speed videos analyzed for each filmed stalagmite. Date(s) at which videos were recorded. Falling heights z_0 between the top of the stalagmites and the tip of their respective corresponding stalactites. Residual film thickness δ on top of the stalagmites. Body average radii s_b of the filmed stalagmites (Fig. 5 of the main text). Top radii s_t of the filmed stalagmites (Fig. 5 of the main text). Hyperlinks to tables summarizing the measurements collected from the high-speed videos relative to each stalagmite: drop radius R, drop impact velocity v_0, dispersal of the drop impact position Δ, and maximum size of the lamella formed at impact r. Hyperlinks to pictures of the stalagmites.

Color	Cave	Stalagmite	z_0 (m)	s_b (cm)	s_t (cm)
●	*Bétharram*	1	6.70	4.66	3.07
		2	2.39	3.36	1.68
●	*Clamouse*	3	7.00	3.74	2.21
		4	1.00	3.42	2.61
		5	0.85	3.40	1.97
		6	3.22	2.86	1.36
		7	4.00	3.74	1.98
		8	1.10	3.40	2.68
		9	0.25	2.38	1.87
		10	0.50	2.65	1.54
		11	3.00	3.24	1.77
		12	3.00	2.85	2.44
		13	0.31	2.75	2.12
		14	0.47	2.62	1.61
		15	0.48	2.78	1.68
		16	0.66	2.91	1.64
		17	2.80	3.30	1.80
		18	0.50	2.22	2.40
		19	0.50	2.63	1.44
		20	0.40	2.67	1.76
		21	0.90	2.38	1.69
●	*Esparros*	22	5.35	4.43	2.80
		23	5.50	4.26	2.76
●	*Gargas*	24	5.20	4.53	2.57
		25	0.99	3.30	1.75
●	*Niaux*	26	2.04	2.76	1.63
		27	4.70	4.09	2.74
●	*Orgnac*	28	22.00	8.36	4.58
		29	5.25	3.83	2.82
		30	7.90	5.69	3.44
		31	5.60	5.20	2.92
		32	10.50	5.75	2.98
		33	24.00	8.85	5.91
		34	27.70	7.95	5.64
		35	26.70	9.42	5.98
		36	11.70	4.99	3.57
		37	11.60	6.65	3.67
		38	12.50	5.84	3.78
		39	11.60	5.63	4.42
		40	22.10	8.89	3.59
●	*La Salamandre*	41	25.70	8.17	5.24
		42	12.70	6.00	3.73
		43	15.10	6.47	2.94
		44	15.00	5.66	3.98
		45	11.80	5.70	3.17
		46	18.70	6.26	3.64
		47	19.50	7.67	3.99
		48	21.40	8.26	4.59
		49	21.20	7.70	5.05
		50	19.70	8.06	5.41
		51	19.30	7.19	5.03

Table S2: Still picture database. Colors associated to the caves in which still pictures of stalagmites were taken. Names of these caves. Falling heights and stalagmite body average radii s_b and top radii s_t of the stalagmites, represented in Fig. 6 of the main text.

Video	R (mm)	v_0 (m/s)	Δ (cm)	r (cm)
1	2.68	8.46	0.81	2.05
2	2.54	8.41	-1.21	2.06
3	2.34	8.85	1.26	2.16
4	2.35	8.30	0.31	2.17
5	2.77	8.72	0.54	1.98
6	2.43	8.51	0.65	2.05
7	2.39	8.89	0.18	2.09
8	2.90	8.93	1.43	1.98
9	2.53	8.77	1.02	2.14
10	3.00	8.61	0.56	2.21
11	2.83	8.51	-0.23	1.78
12	2.41	8.61	-0.64	1.87
13	2.48	8.29	0.44	1.71
14	2.27	8.45	-0.39	1.64
15	2.71	8.36	2.62	1.53
16	2.44	8.09	2.45	2.13
17	2.59	8.57	0.51	2.03
18	2.92	8.67	-0.21	2.15
19	2.83	9.07	1.96	1.37
20	2.43	8.74	-0.69	1.68
21	2.37	8.83	2.66	1.95
22	2.29	8.53	-1.25	1.65
23	2.38	8.86	1.39	2.11
24	2.43	8.63	-0.94	1.46
25	2.87	8.74	2.87	1.60
26	2.67	8.51	-1.93	1.39
27	2.49	8.29	0.41	2.25
28	2.50	8.86	0.57	2.15
29	2.50	8.43	-0.07	1.96
30	2.71	8.94	2.39	1.61
31	2.57	8.83	0.87	1.76
32	2.28	8.59	0.36	2.32
33	1.82	8.67	-1.45	1.47
34	2.90	8.88	-0.26	1.91
35	2.39	8.78	0.32	2.20
36	2.34	8.76	-1.30	1.58
37	2.77	8.37	0.14	1.73
38	2.55	8.14	-0.10	2.06
39	3.34	8.56	-0.04	2.06
40	2.46	8.73	2.49	2.16
41	2.60	8.29	-0.96	1.95
42	2.54	8.77	1.45	1.83
43	2.90	8.35	1.26	2.10
44	2.52	8.19	0.82	1.91
45	2.59	8.58	-0.57	1.72
46	2.63	8.25	1.09	2.11
47	3.04	8.69	1.50	2.03
48	2.71	8.61	0.81	2.02
49	2.35	8.29	-1.83	1.57
50	3.02	8.40	3.60	1.78

Table S3. Measurements from all high-speed videos analyzed for stalagmite Clam01 ● (see Table S1): drop radius R, drop impact velocity v_0, dispersal of the drop impact position Δ, maximum size of the lamella formed at impact r.

Video	R (mm)	v_0 (m/s)	Δ (cm)	r (cm)
1	2.87	4.40	0.28	1.32
2	2.85	4.42	0.36	0.89
3	2.82	4.42	0.49	1.56
4	2.84	4.40	0.01	1.42
5	2.82	4.42	-0.18	1.18
6	2.84	4.45	0.04	1.31
7	2.84	4.40	0.10	0.94
8	2.80	4.37	-0.09	2.18
9	2.82	4.42	0.15	0.81
10	2.81	4.42	0.32	1.02
11	2.83	4.45	0.20	0.90
12	2.84	4.45	-0.02	1.02
13	2.82	4.40	0.28	0.89
14	2.86	4.42	0.03	0.88
15	2.80	4.42	0.43	0.75
16	2.81	4.45	0.28	0.73
17	2.81	4.45	0.29	0.83
18	2.85	4.42	0.29	0.80
19	2.83	4.42	0.04	0.99
20	2.85	4.40	-0.02	1.06
21	2.88	4.42	0.10	1.14
22	2.85	4.42	-0.56	1.11
23	2.88	4.42	0.03	0.99
24	2.88	4.40	0.12	1.05
25	2.88	4.42	-0.10	1.09
26	2.97	4.42	0.21	1.08
27	2.87	4.42	-0.20	1.01
28	2.88	4.40	-0.13	1.31
29	2.86	4.37	0.03	1.29
30	2.87	4.40	-0.11	1.46
31	2.88	4.40	-0.07	1.36
32	2.86	4.42	0.21	1.49
33	2.88	4.42	0.05	1.27
34	2.87	4.42	0.17	1.36
35	2.84	4.40	-0.17	1.27
36	2.86	4.42	0.01	1.32
37	2.89	4.42	-0.17	1.36
38	2.88	4.40	0.05	1.37
39	2.87	4.40	-0.01	1.51
40	2.89	4.40	0.10	1.42
41	2.85	4.40	-0.08	1.21
42	2.85	4.40	0.04	1.36
43	2.84	4.37	-0.18	1.54
44	2.87	4.40	-0.39	1.17
45	2.88	4.42	0.10	1.21
46	2.89	4.42	0.16	1.48
47	2.84	4.42	-0.16	1.56
48	2.85	4.40	-0.04	1.42
49	2.83	4.37	-0.11	1.18
50	2.87	4.37	-0.09	1.31

Table S4. Measurements from all high-speed videos analyzed for stalagmite Clam02 ■ (see Table S1): drop radius R, drop impact velocity v_0, dispersal of the drop impact position Δ, maximum size of the lamella formed at impact r.

Video	R (mm)	v_0 (m/s)	Δ (cm)	r (cm)
1	2.31	2.54	-0.26	1.45
2	2.49	2.36	0.53	1.61
3	2.42	2.43	0.50	1.49
4	2.73	2.48	0.56	1.54
5	2.26	2.35	0.50	1.66
6	2.56	2.56	0.26	1.46
7	2.60	2.42	-0.06	1.63
8	2.59	2.42	-0.12	1.51
9	2.61	2.49	-0.15	1.59
10	2.63	2.29	-0.06	1.67

Table S5. Measurements from all high-speed videos analyzed for stalagmite Clam03 ♦ (see Table S1) drop radius R, drop impact velocity v_0, dispersal of the drop impact position Δ, maximum size of the lamella formed at impact r.

Video	R (mm)	v_0 (m/s)	Δ (cm)	r (cm)
1	2.89	7.40	-0.13	–
2	2.65	7.42	0.43	–
3	2.69	7.54	-0.49	–
4	2.81	7.26	-0.50	–
5	2.76	7.16	0.12	–
6	2.68	7.50	0.31	–
7	2.80	6.98	0.26	–

Table S6. Measurements from all high-speed videos analyzed for stalagmite Org07 ◀ (see Table S1): drop radius R, drop impact velocity v_0, dispersal of the drop impact position Δ, maximum size of the lamella formed at impact r.

Video	R (mm)	v_0 (m/s)	Δ (cm)	r (cm)
1	2.91	9.79	-0.36	2.36
2	2.76	9.79	3.82	2.28
3	2.62	9.47	-8.21	–
4	2.74	9.79	-4.15	–
5	2.69	9.51	4.26	–
6	2.74	9.14	-5.00	–
7	2.65	9.14	-3.76	2.28
8	2.76	9.64	0.94	–
9	2.88	9.32	4.45	2.28
10	2.81	9.79	-1.65	2.39
11	2.80	9.29	5.32	–
12	2.94	9.52	5.40	2.56
13	3.03	9.45	-6.44	2.28
14	2.67	9.69	3.33	2.23
15	2.83	9.14	-1.65	2.38
16	2.87	9.52	-4.16	–
17	2.95	10.04	-0.98	2.25
18	2.49	9.46	0.68	2.40
19	2.71	9.22	2.91	–
20	2.55	–	–	–
21	2.77	–	–	2.11
22	2.53	–	–	–
23	2.75	9.44	-1.35	2.36
24	2.50	9.36	-1.28	2.39
25	2.86	9.91	4.43	–
26	2.68	9.28	-1.27	2.08
27	2.64	9.44	1.14	2.06

Table S7. Measurements from all high-speed videos analyzed for stalagmite Org02 ■ (see Table S1): drop radius R, drop impact velocity v_0, dispersal of the drop impact position Δ, maximum size of the lamella formed at impact r.

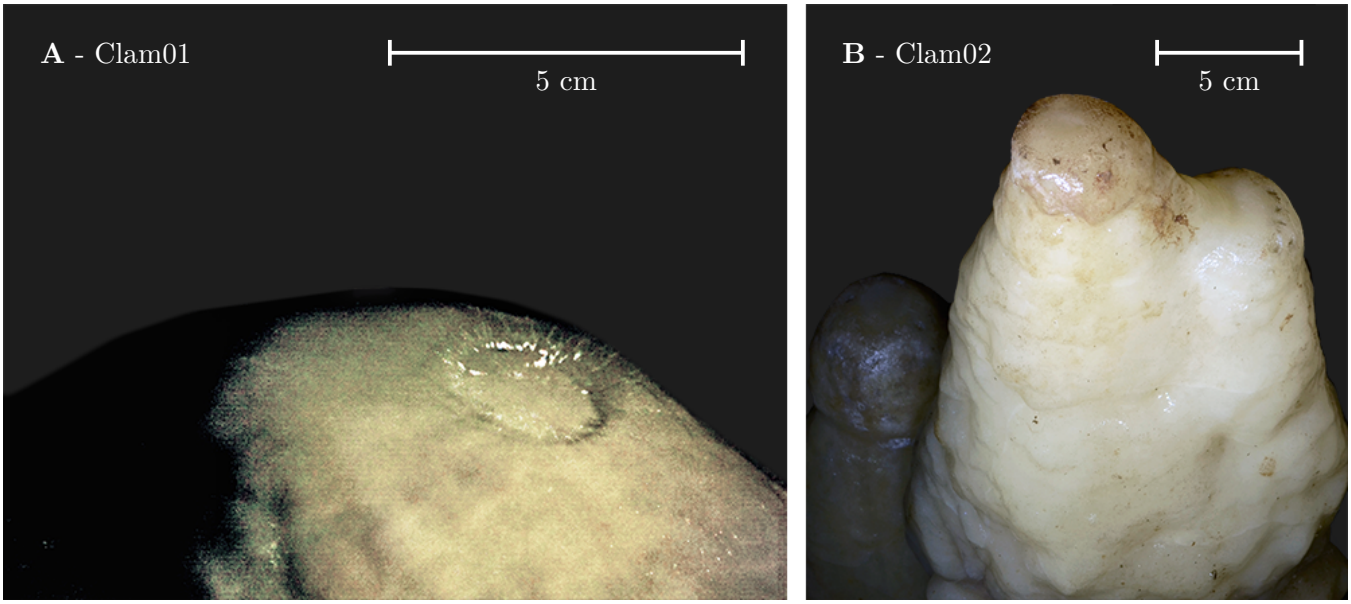

Fig. S7. A - A drop impacting Clam01 ●, Clamouse cave, salle rouge. Picture was taken 600 μs after the drop impact. **B** - Picture of Clam02 ■, Clamouse cave, Cimetière.

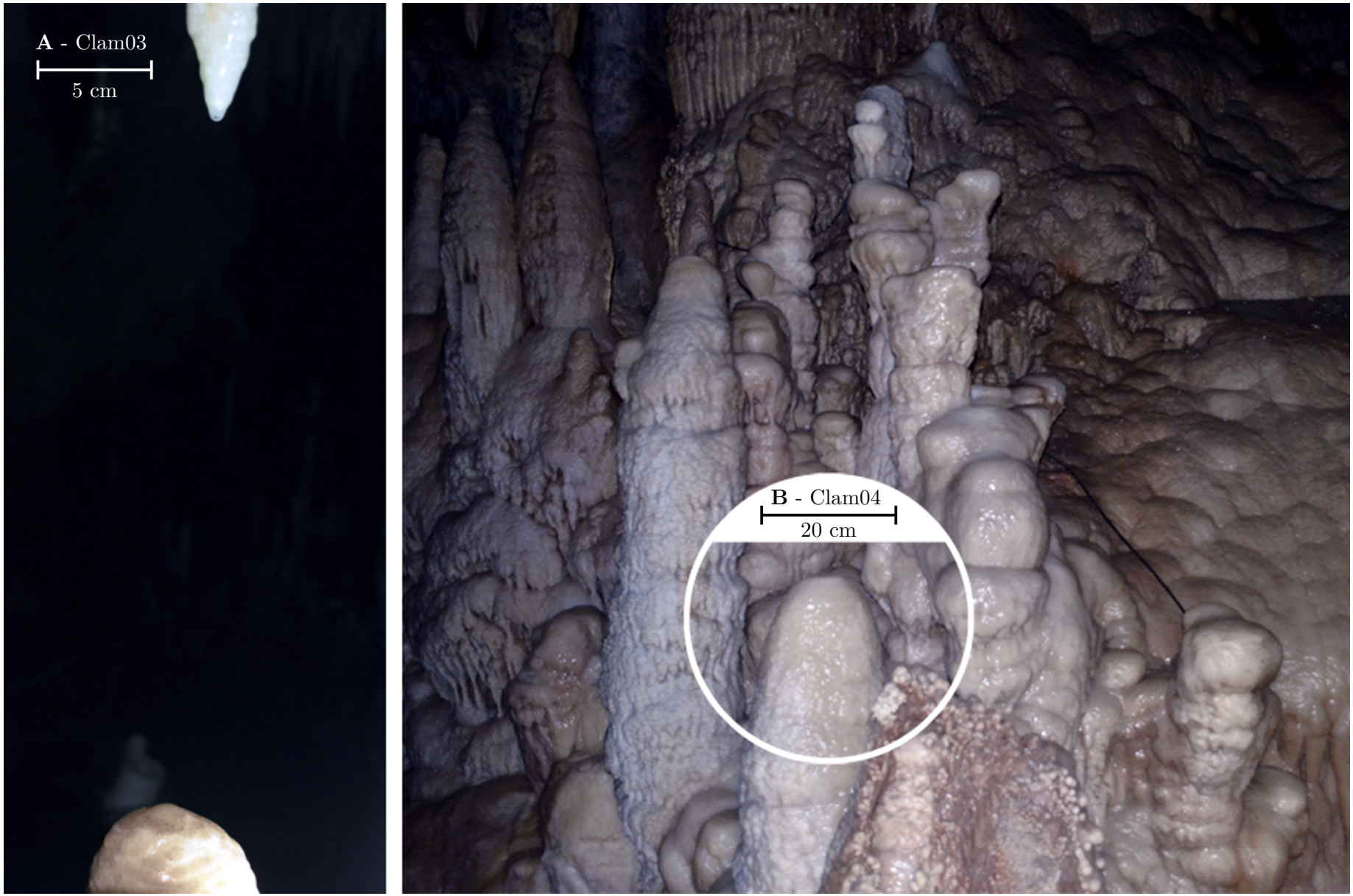

Fig. S8. A - Picture of Clam03 ♦ along with the above stalactite, Clamouse cave, Cimetière. **B** - Picture of Clam04 ▼, Clamouse cave, below Cimetière.

Video	R (mm)	v_0 (m/s)	Δ (cm)	r (cm)
1	2.65	8.99	0.95	1.52
2	2.53	8.74	0.38	1.48
3	2.36	8.74	0.27	1.57
4	2.22	8.24	-0.83	1.78
5	2.55	8.68	-1.22	1.43
6	2.41	8.55	2.94	1.42
7	2.42	8.99	1.02	1.58
8	2.50	8.68	3.73	1.44
9	2.45	8.43	0.23	1.88
10	2.54	8.55	-1.24	1.87
11	2.63	8.87	1.57	1.89
12	2.44	8.49	-1.31	2.12
13	2.46	8.74	-0.10	1.86
14	2.67	8.68	3.48	1.63
15	2.48	8.68	2.74	2.57
16	2.33	8.61	4.85	2.57
17	2.56	8.55	-0.52	1.87
18	2.35	8.74	-0.52	1.69
19	2.70	8.93	0.93	1.95
20	2.79	8.37	-1.59	1.45
21	2.37	8.43	0.83	1.69
22	2.44	9.05	2.16	1.18
23	2.83	8.61	0.02	1.61
24	2.20	8.55	2.71	1.44
25	2.28	8.24	-0.28	1.57
26	2.54	8.30	0.37	1.26
27	2.29	8.80	0.03	1.46
28	2.39	8.93	2.11	1.37
29	2.45	8.74	-1.66	1.57
30	2.46	8.86	-0.58	1.63
31	2.63	8.80	-0.04	1.37
32	2.28	8.36	-1.85	1.52
33	2.47	8.43	0.45	1.34
34	2.42	9.44	3.48	-
35	2.50	8.55	0.44	1.28
36	2.25	8.49	1.71	1.28
37	2.55	8.99	2.41	1.38
38	2.71	8.86	0.37	1.64
39	2.62	8.92	1.19	1.36
40	2.39	8.55	0.84	1.28
41	2.61	8.18	0.42	1.76
42	2.30	8.37	-1.61	1.59
43	2.62	8.86	-2.63	1.35
44	2.48	8.99	3.24	1.75
45	2.70	8.43	-0.01	1.30
46	2.64	8.86	1.10	1.56
47	2.63	8.68	-0.17	1.60
48	2.43	8.49	1.65	1.92
49	2.69	8.99	0.66	1.71

Table S8. Measurements from all high-speed videos analyzed for stalagmite Clam04 ▼ (see Table S1): drop radius R, drop impact velocity v_0, dispersal of the drop impact position Δ, maximum size of the lamella formed at impact r.

Video	R (mm)	v_0 (m/s)	Δ (cm)	r (cm)
1	2.65	8.99	0.95	2.29
2	2.53	8.74	0.38	2.41
3	2.57	8.74	0.27	-
4	2.39	8.24	-0.83	2.45
5	2.55	8.68	-1.22	1.72
6	2.53	8.55	2.94	1.59
7	2.45	8.99	1.02	1.60
8	2.62	8.68	3.73	2.41
9	2.45	8.43	0.23	2.41
10	2.54	8.55	-1.24	2.00
11	2.53	8.87	1.57	2.10
12	2.44	8.49	-1.31	2.29
13	2.46	8.74	-0.10	2.29
14	2.67	8.68	3.48	2.28
15	2.48	8.68	2.74	2.29
16	2.49	8.61	4.85	-
17	2.56	8.55	-0.52	2.31
18	2.50	8.74	-0.52	2.31
19	2.57	8.93	0.93	2.26
20	2.63	8.37	-1.59	2.34
21	2.49	8.43	0.83	2.46
22	2.44	9.05	2.16	1.51
23	2.50	8.61	0.02	1.59
24	2.49	8.55	2.71	1.60
25	2.58	8.24	-0.28	2.34
26	2.54	8.30	0.37	2.52
27	2.47	8.80	0.03	2.48
28	2.39	8.93	2.11	2.00
29	2.45	8.74	-1.66	2.10
30	2.69	8.54	4.48	2.11
31	2.24	8.25	-5.92	2.29
32	2.60	8.23	0.25	1.69
33	2.77	9.04	1.08	1.56
34	2.54	8.30	2.03	2.43
35	2.67	8.48	-4.28	2.29
36	2.69	8.54	3.87	2.23
37	2.79	8.81	0.19	2.43
38	2.65	8.35	1.17	2.37
39	2.68	9.08	4.29	1.51
40	2.91	8.85	1.73	1.59
41	2.83	9.08	3.87	1.60
42	2.88	8.89	1.08	2.41
43	2.87	9.10	3.53	2.48
44	2.64	8.85	2.18	2.16
45	2.59	8.66	1.45	2.03
46	2.73	9.02	7.32	1.61
47	2.75	8.48	0.55	2.49
48	2.81	8.86	-2.42	1.91
49	2.50	8.47	1.15	2.11
50	2.70	8.61	-0.67	2.11
51	2.63	9.28	1.76	2.03
52	2.38	8.60	-6.12	1.66
53	2.73	9.73	0.03	2.03
54	2.81	9.08	-1.44	1.78
55	2.80	9.02	0.13	2.60
56	2.30	8.40	-1.46	1.82

Table S9. Measurements from all high-speed videos analyzed for stalagmite Org01 ● (see Table S1): drop radius R, drop impact velocity v_0, dispersal of the drop impact position Δ, maximum size of the lamella formed at impact r.

Video	R (mm)	v_0 (m/s)	Δ (cm)	r (cm)
1	2.52	6.26	0.36	–
2	2.57	6.29	0.04	–
3	2.70	6.39	-0.01	–
4	2.60	6.30	-0.10	–
5	2.59	6.42	0.31	–
6	2.61	6.65	-0.12	–
7	2.41	6.30	-0.35	–
8	2.73	6.42	-0.19	–
9	2.63	6.33	-0.10	–
10	2.73	6.26	-0.03	–
11	2.48	6.33	0.08	–
12	2.74	6.42	-0.16	–
13	2.62	6.27	-0.14	–
14	2.71	6.42	0.02	–
15	2.76	6.42	0.04	–
16	2.72	6.29	0.03	–
17	2.55	6.36	-0.08	–
18	2.55	6.36	-0.08	–
19	2.56	6.46	0.18	–
20	2.75	6.39	-0.15	–
21	2.47	6.61	-0.16	–
22	2.40	6.39	0.01	–
23	2.67	6.32	0.12	–
24	2.69	6.39	0.03	–
25	2.76	6.35	0.05	–
26	2.35	6.61	0.09	–
27	2.69	6.30	0.14	–
28	2.73	6.40	0.24	–
29	2.53	6.36	-0.01	–
30	2.60	6.30	-0.05	–
31	2.44	6.39	0.01	–
32	2.73	6.21	–	–
33	2.73	6.29	0.04	–
34	2.41	6.36	0.16	–
35	2.62	6.42	0.22	–
36	2.75	6.32	0.15	–
37	2.71	6.45	0.18	–
38	2.72	6.30	-0.07	–
39	2.65	6.30	-0.15	–
40	2.58	6.42	-0.06	–
41	2.51	6.36	-0.01	–
42	2.62	6.39	0.16	–
43	2.67	6.36	0.06	–
44	2.62	6.61	-0.22	–
45	2.72	6.33	0.11	–
46	2.71	6.36	-0.01	–
47	2.61	6.27	-0.20	–
48	2.47	6.68	-0.40	–
49	2.54	6.39	0.05	–
50	2.63	6.26	-0.03	–

Table S10. Measurements from all high-speed videos analyzed for stalagmite Org03 ♦ (see Table S1): drop radius R, drop impact velocity v_0, dispersal of the drop impact position Δ, maximum size of the lamella formed at impact r.

Video	R (mm)	v_0 (m/s)	Δ (cm)	r (cm)
1	–	7.15	-1.55	–
2	2.51	6.72	1.34	0.89
3	–	6.91	-0.89	–
4	–	6.83	-0.87	–
5	2.73	6.85	1.46	–
6	2.54	6.86	1.29	0.93
7	–	7.10	-1.95	–
8	–	7.45	-1.82	–
9	–	7.16	-2.22	–
10	2.56	7.71	1.61	0.96
11	–	7.37	-1.48	–
12	–	7.20	-2.16	–
13	–	7.28	-2.37	–
14	–	6.73	-1.23	–
15	–	7.28	-1.34	–
16	2.68	7.10	-1.85	0.96
17	–	7.01	-1.46	–
18	2.57	6.96	1.45	–
19	2.47	7.10	0.71	1.00
20	2.66	7.19	1.12	0.93
21	2.77	7.06	-1.92	0.90
22	–	6.95	-1.19	–
23	–	7.17	-2.07	–
24	–	7.28	-1.95	–
25	–	7.28	-2.53	–
26	2.51	6.83	1.11	1.03
27	–	7.01	-1.07	–
28	2.57	6.91	1.44	1.00
29	2.59	7.01	1.39	1.02
30	–	7.48	-1.29	–
31	2.59	6.77	1.47	–
32	2.46	6.93	1.53	1.12
33	2.38	7.20	0.33	1.05
34	2.69	6.72	1.29	–
35	–	7.11	-2.01	–
36	–	6.82	-1.04	–
37	–	7.29	-1.21	–
38	2.74	6.91	1.43	0.93
39	2.57	6.85	1.29	–
40	2.47	7.01	1.59	–
41	2.66	7.10	1.39	0.87
42	2.44	6.68	0.99	0.91
43	2.53	6.95	1.29	0.99
44	2.66	6.94	1.12	–
45	2.42	6.82	1.28	1.00
46	2.48	7.10	0.18	1.10
47	2.49	6.79	1.69	–
48	–	6.96	-1.25	–

Table S11. Measurements from all high-speed videos analyzed for stalagmite Org04 ▼ (see Table S1): drop radius R, drop impact velocity v_0, dispersal of the drop impact position Δ, maximum size of the lamella formed at impact r.

Video	R (mm)	v_0 (m/s)	Δ (cm)	r (cm)
1	2.62	8.49	3.86	2.10
2	2.44	8.18	0.55	–
3	2.96	9.49	5.42	2.23
4	2.86	9.79	6.09	1.85
5	2.42	9.41	7.97	–
6	2.51	9.26	12.61	–
7	2.52	9.37	9.34	–
8	2.71	9.37	6.52	2.12
9	3.01	9.49	2.25	2.14
10	2.80	8.69	2.97	1.85
11	2.96	9.12	5.18	2.29
12	2.46	9.02	6.89	2.16
13	2.31	8.62	5.50	–
14	2.62	8.93	1.52	2.43
15	2.56	8.11	6.33	–
16	2.41	9.24	6.05	2.27
17	2.93	8.90	3.87	2.56
18	2.85	9.13	3.66	2.35
19	2.97	8.69	2.37	2.05
20	2.90	9.79	2.21	2.13
21	2.39	9.28	4.52	2.28
22	2.61	8.49	2.90	2.57
23	2.53	8.36	3.25	2.64
24	2.45	8.72	1.26	–
25	2.50	9.03	5.44	2.20
26	2.43	8.31	-4.07	–
27	2.53	8.10	2.59	–
28	2.95	9.39	2.34	2.04
29	2.90	9.29	2.86	2.59
30	2.69	8.24	1.04	2.24
31	2.88	9.20	2.36	2.52
32	2.85	9.53	3.67	1.82
33	2.40	8.73	3.82	2.28
34	2.33	8.36	4.20	2.22
35	2.27	9.00	2.76	2.41
36	2.64	9.11	2.39	2.35
37	2.61	8.86	-0.42	2.54
38	2.36	8.58	7.58	–
39	2.57	8.14	4.08	–
40	2.65	8.88	2.45	2.38
41	2.82	9.14	3.54	2.51
42	2.69	8.86	1.51	–
43	2.49	9.00	-0.32	2.16
44	2.55	8.74	5.31	2.21
45	2.34	9.03	5.47	2.05
46	2.57	8.24	5.01	–
47	2.60	8.47	1.50	–
48	2.32	8.25	2.59	2.44
49	2.72	9.63	9.75	–
50	2.32	9.10	1.81	–

Table S12. Measurements from all high-speed videos analyzed for stalagmite Org05 ▲ (see Table S1): drop radius R, drop impact velocity v_0, dispersal of the drop impact position Δ, maximum size of the lamella formed at impact r.

Video	R (mm)	v_0 (m/s)	Δ (cm)	r (cm)
1	–	9.04	-1.26	–
2	2.75	9.40	1.29	1.51
3	–	8.93	-3.62	–
4	–	8.70	1.35	–
5	2.88	9.02	-11.67	–
6	–	8.63	-3.31	–
7	–	8.89	0.98	–
8	2.61	9.59	-7.23	1.51
9	2.80	9.23	-1.88	1.58
10	2.60	9.14	2.03	1.65
11	–	8.91	-2.32	–
12	2.83	9.40	-1.51	2.02
13	–	8.89	-3.72	–
14	–	9.00	0.54	–
15	–	8.39	-5.15	–
16	–	8.68	-5.18	–
17	2.80	9.04	-4.46	–
18	2.78	9.14	-1.42	–
19	–	9.35	6.20	–
20	–	8.70	-2.13	–
21	–	8.96	-0.58	–
22	–	8.75	-2.26	–
23	2.76	9.38	-0.70	1.62
24	2.80	9.19	-7.07	–
25	2.81	9.50	-3.31	1.91
26	–	8.77	-4.49	–
27	–	8.77	-5.55	–
28	2.74	9.29	-3.87	1.91
29	–	8.98	-4.96	–
30	–	9.38	6.88	–
31	–	9.17	0.04	–
32	–	9.12	0.14	–
33	–	8.93	-2.94	–
34	2.79	9.04	-4.59	1.93
35	–	9.02	1.38	–
36	–	9.29	10.79	–
37	2.58	9.42	2.53	1.95
38	–	8.87	-1.73	–
39	2.71	9.50	1.32	2.10
40	2.64	9.25	1.72	1.70
41	–	9.04	1.85	–
42	–	8.93	0.79	–

Table S13. Measurements from all high-speed videos analyzed for stalagmite Org06 ▶ (see Table S1): drop radius R, drop impact velocity v_0, dispersal of the drop impact position Δ, maximum size of the lamella formed at impact r.

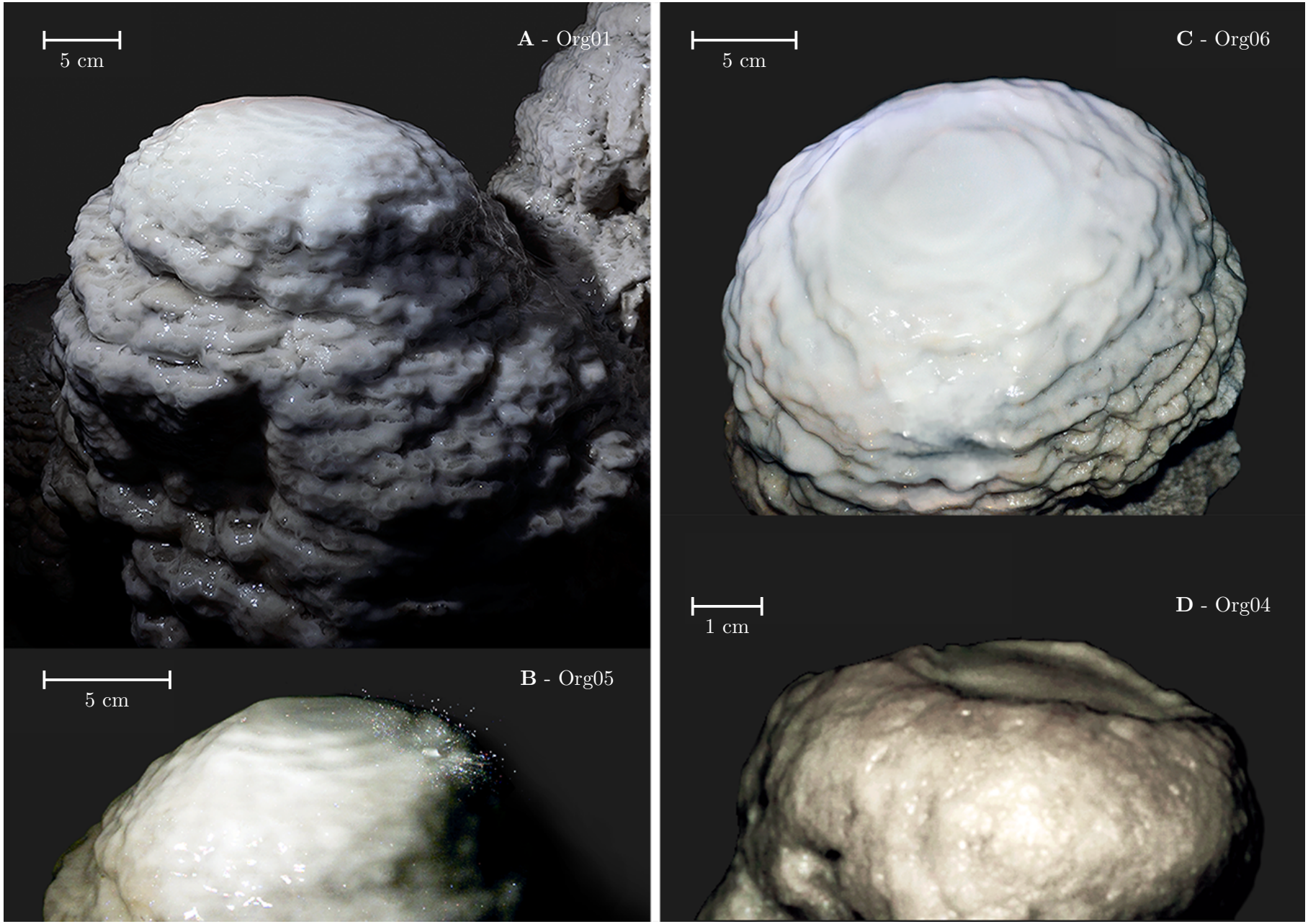

Fig. S9. A - Picture of Org01 ●, Orgnac cave, salle de Joly, near the Tour de Pise concretion. **B** - Superimposition of 8 frames (by stack projection) of a drop impacting Org05 ▲, Orgnac cave, near the Blocs cyclopéens concretion. The frames are separated by 200 μs. **C** - Picture of Org06 ▶, Orgnac cave, near the Cône d'éboulis concretion. **D** - Picture of Org04 ▼, Orgnac cave, near salle Glory.

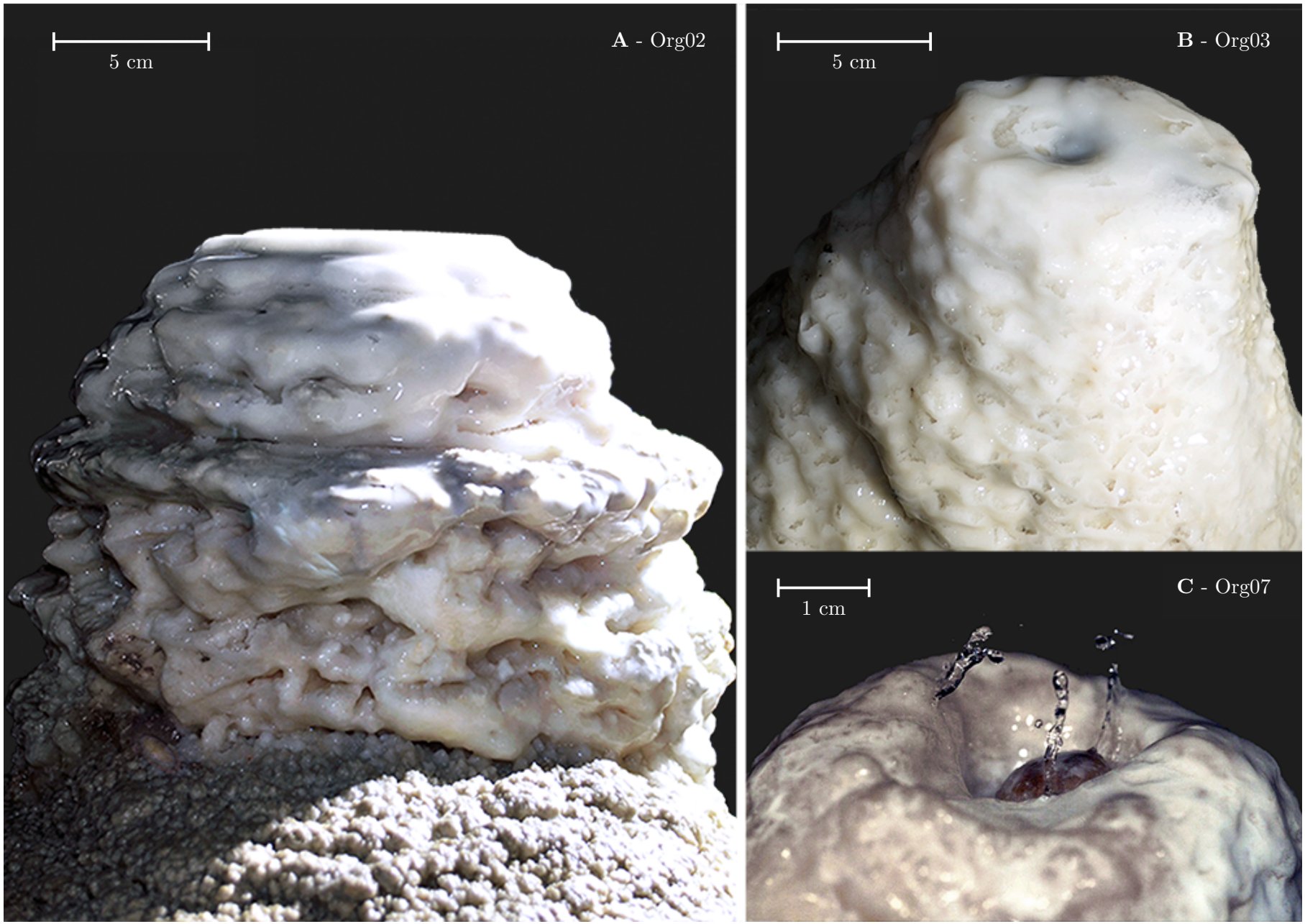

Fig. S10. A - Picture of Org02 ■, Orgnac cave, salle de Joly, near the Pomme de pin concretion. **B** - Picture of Org03 ♦, Orgnac cave, in salle de Joly near the entrance of salle Glory. **C** - Picture of a splashing drop impacting Org07 ◀, Orgnac cave, salle Glory. Picture was taken 15 ms after the drop impact.

Video	R (mm)	v_0 (m/s)	Δ (cm)	r (cm)
1	2.53	8.98	7.86	1.61
2	2.46	8.98	7.76	1.68
3	2.60	8.52	-4.98	1.34
4	2.70	9.03	4.21	1.84
5	2.74	9.12	-0.86	1.81
6	2.43	8.94	-1.96	1.37
7	2.58	9.15	-2.26	1.51
8	2.45	9.16	-2.13	1.97
9	2.53	8.70	-1.12	–
10	2.48	8.47	4.21	1.57
11	2.48	9.24	-7.66	–
12	2.53	8.82	-1.46	–
13	2.68	8.63	-2.08	–
14	2.83	9.25	1.11	1.79
15	2.42	9.01	1.06	1.74
16	2.71	8.70	0.04	–
17	2.39	8.93	0.43	–
18	2.40	9.01	2.03	1.63
19	2.75	9.09	-1.07	1.71
20	2.69	9.15	-1.67	1.97
21	2.46	8.63	7.42	1.64
22	2.79	9.24	5.84	1.57
23	2.24	9.14	-5.75	1.80
24	2.32	9.30	5.04	1.56
25	2.47	9.01	3.78	–
26	2.55	8.70	0.83	–
27	2.59	8.76	1.34	–
28	2.52	8.70	0.37	–
29	2.30	8.86	-1.60	1.51
30	2.39	8.39	0.17	–
31	2.51	8.86	6.38	–
32	2.47	8.96	0.49	1.51
33	2.69	9.25	4.31	1.97
34	2.61	9.17	-1.28	–
35	2.53	9.12	0.63	1.57
36	2.74	8.47	-7.24	–
37	2.54	9.40	2.08	1.89
38	2.64	9.11	-0.72	1.96
39	2.46	9.16	3.42	1.75
40	2.46	8.70	2.86	1.74
41	2.72	9.24	-3.06	1.70
42	2.55	9.09	4.20	1.68
43	2.77	8.71	2.91	1.63

Table S14. Measurements from all high-speed videos analyzed for stalagmite Sal01 ● (see Table S1): drop radius R, drop impact velocity v_0, dispersal of the drop impact position Δ, maximum size of the lamella formed at impact r.

Video	R (mm)	v_0 (m/s)	Δ (cm)	r (cm)
1	2.40	8.93	0.29	2.40
2	2.66	9.05	2.90	2.66
3	2.93	9.62	2.29	2.93
4	2.41	8.73	2.89	2.41
5	2.72	8.78	-1.58	2.72
6	2.75	8.65	1.22	2.75
7	2.34	9.17	0.35	2.34
8	2.52	9.00	1.50	2.52
9	2.64	8.54	2.69	2.64
10	2.84	9.22	0.51	2.84
11	2.59	9.28	0.92	2.59
12	2.34	8.61	4.94	2.34
13	2.71	9.13	-1.88	2.71
14	2.69	9.23	-3.70	2.69
15	2.76	8.49	-4.07	2.76
16	2.70	9.69	-1.54	2.42
17	2.88	9.53	1.31	1.99
18	2.74	9.80	0.46	2.21
19	2.54	8.73	6.16	2.00
20	2.62	8.80	-1.66	2.32
21	2.69	9.43	6.11	1.99
22	2.84	9.81	4.23	2.23
23	3.03	9.21	4.25	1.97
24	–	9.46	6.16	–
25	2.72	9.78	-3.12	2.11
26	2.79	9.86	0.13	2.48
27	2.83	9.31	7.05	2.14
28	2.76	9.03	-3.52	–
29	2.87	9.18	1.66	2.32
30	2.74	9.65	3.71	2.01
31	2.72	9.25	5.26	2.20
32	2.85	9.39	6.58	–
33	2.98	9.92	5.43	–
34	2.75	8.90	3.52	2.16
35	2.91	9.96	2.44	2.41
36	2.88	9.44	3.45	2.38
37	2.72	9.37	5.78	1.97
38	2.85	9.70	-0.01	2.09
39	2.78	9.79	0.72	2.22
40	2.79	9.45	-0.86	2.31
41	2.79	9.30	5.67	2.07
42	2.70	8.79	4.96	2.22
43	–	8.46	-4.01	–
44	2.60	9.42	-1.89	2.21
45	2.77	10.08	-1.26	2.25
46	2.42	8.32	2.09	2.00
47	2.65	9.22	-0.55	2.37
48	2.80	9.55	0.23	2.54
49	2.59	9.06	3.59	2.34
50	2.52	8.97	-3.87	2.24

Table S15. Measurements from all high-speed videos analyzed for stalagmite Sal02 ■ (see Table S1): drop radius R, drop impact velocity v_0, dispersal of the drop impact position Δ, maximum size of the lamella formed at impact r.

Video	R (mm)	v_0 (m/s)	Δ (cm)	r (cm)
1	2.52	8.53	1.55	2.04
2	2.41	9.11	3.70	1.74
3	2.76	9.02	1.45	2.16
4	2.74	9.09	0.76	2.11
5	2.44	8.85	2.82	2.17
6	2.69	9.15	3.45	1.74
7	2.78	9.01	1.70	2.04
8	2.58	8.61	2.68	2.17
9	2.39	9.15	3.47	–
10	2.78	8.65	0.82	–
11	2.43	9.16	-2.61	2.04
12	2.42	8.43	-0.91	1.90
13	2.42	8.60	-0.85	–
14	2.25	9.01	3.41	2.05
15	2.71	8.67	3.57	2.17
16	2.32	8.61	-0.45	2.04
17	2.77	9.03	3.74	1.89
18	2.70	9.11	4.48	2.16
19	2.65	8.94	0.90	2.16
20	2.70	8.87	5.60	2.17
21	2.52	8.87	2.83	1.90
22	2.62	8.90	4.27	1.91
23	2.49	9.15	4.02	2.17
24	2.55	8.46	0.51	1.75
25	2.65	8.69	0.26	1.73
26	2.38	8.43	0.96	2.04
27	2.78	9.04	0.46	1.69
28	2.76	9.12	0.35	2.04
29	2.66	8.31	1.72	2.27
30	2.76	9.05	0.73	2.04
31	2.43	8.36	0.69	2.15
32	2.44	9.02	0.17	1.92
33	2.78	9.06	1.94	–
34	2.70	8.62	3.06	2.04
35	2.45	9.07	1.00	1.79
36	2.46	8.79	2.43	–
37	2.10	9.33	3.62	2.04
38	2.90	8.79	1.40	1.89
39	2.54	8.67	-0.85	2.16
40	2.73	9.10	2.32	2.16
41	2.76	9.05	0.66	2.17
42	2.52	9.11	4.57	1.70
43	2.85	8.81	-0.18	1.91
44	2.61	8.54	3.04	2.17
45	2.44	8.73	3.14	1.83
46	2.53	9.18	0.96	1.66
47	2.75	8.91	2.37	1.96
48	2.73	8.55	-0.99	1.99
49	2.53	8.39	-0.12	1.77
50	2.58	9.07	1.12	2.04

Table S16. Measurements from all high-speed videos analyzed for stalagmite Sal03 ♦ (see Table S1): drop radius R, drop impact velocity v_0, dispersal of the drop impact position Δ, maximum size of the lamella formed at impact r.

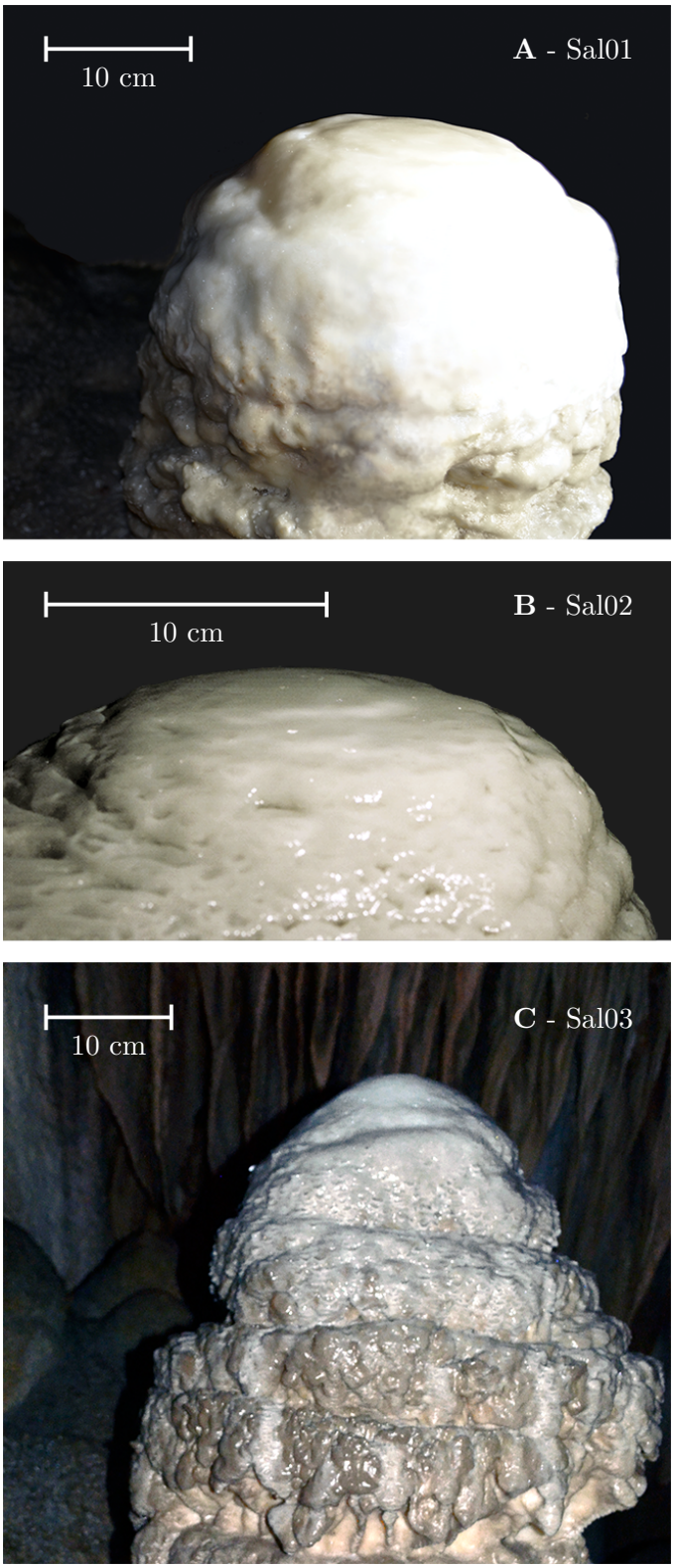

Fig. S11. **A** - Picture of Sal01 ●, La Salamandre cave, near the Pomme de pin concretion. **B** - Picture of Sal02 ■, La Salamandre cave, near the Cierges concretion. **C** - Picture of Sal03 ♦, La Salamandre cave, near the Grands Massifs concretion.